JOURNAL OF SOLID STATE CHEMISTRY 11, 38–52 (1974)

Characterization of Paramagnetic Hole-Centers in Al_2O_3 and Al_2O_3:Fe by Optical and EPR Absorption*

C. F. BAUER† AND D. H. WHITMORE

Department of Materials Science, Northwestern University, Evanston, Illinois 60201

Received August 2, 1973

The electron paramagnetic resonance (EPR) and optical absorption spectra of nominally pure and Fe-doped single crystals of Al_2O_3 have been examined before and after gamma-ray irradiation at 77°K. The EPR spectra for doped and irradiated crystals were found to be a function of the iron concentration. Analysis of the optical and EPR spectra observed on the same Fe-doped crystals which had been subjected to gamma-ray irradiations suggests that the center which accounts most satisfactorily for the details of these spectra is: a single trapped-hole localized on an anion which is adjacent to a substitutional divalent iron impurity atom. The optical absorption band ascribed to this center occurs at 3.08 eV.

Introduction

Point imperfections have long been known to exert a strong influence on the physical properties of many crystalline solids. Since such structural defects in most crystalline compounds have a real or virtual charge, subsequent irradiation of materials containing point imperfections has shown that these point defects may act as trapping sites for the electrons and holes freed during the irradiation process (*1*).

Two experimental techniques, optical absorption and electron paramagnetic resonance (EPR), have been found to be relatively well suited for the study of these types of defects. In the case of alkali halides, these techniques have led to a significantly better understanding of the electronic properties and the defect structure of many defect centers occurring in these materials.

* Work supported by the U.S. Office of Naval Research. This work is based in part on a thesis submitted by C. F. Bauer for the Ph.D. degree at Northwestern University, June 1973.

† Now with the Universal Oil Products, Des Plaines, Illinois 60616.

An extension of these techniques to oxide materials generally has not been as rewarding as in the case of alkali halides; the additional trapping potential of the oxygen vacancies, the multivalence of the host ions, and the variety of the crystal structures possible in some oxides provide many complexities not normally found when working with the alkali halides. Moreover, most oxide materials have been found to be relatively resistant to defect production by simple ionizing radiation so that heavy particle irradiations have been required in order to induce significant concentrations of these defects in oxide materials.

Several electron paramagnetic resonance (EPR) experiments on Al_2O_3 specimens which had been subjected to ionizing radiation have been reported in the literature. In particular, Lambe and Kikuchi (*2*) have reported that V^{3+} is converted to V^{2+} by X-ray irradiation of vanadium-doped sapphire. The nature of the underlying defect mechanism responsible for this conversion, however, could not be determined by these investigators. Similarly, Hoskins and Soffer (*3*) reported the observance of a EPR resonance line at liquid helium

temperatures when their samples were subjected to radiation from a high pressure mercury arc lamp. An additional spin resonance line appeared having a g-value characteristic of a hole-center resonance and disappeared when their samples were warmed to room temperature. Gamma-ray irradiation of nominally pure, Verneuil-grown Al_2O_3 single crystals has been investigated at liquid nitrogen temperature by Gamble et al. (*4*). These investigators reported that, after irradiation, a single, asymmetric paramagnetic resonance absorption is observed having an anisotropic g-value slightly greater than the free electron g-value, and they suggested that the resonance line may be due to two types of defect centers: the first is described as an electron trapped at an oxygen vacancy, while the second is described as a hole center localized at an anion next to a charge-deficient cation site. These investigators suggested that this cation site might either be vacant or may contain a monovalent or divalent substitutional impurity.

Optical absorption measurements of Al_2O_3 specimens which had been subjected to ionizing radiations have also been reported in the literature. Levy (*5*, *6*) has examined gamma-ray irradiated alumina grown by a Verneuil process and observed the formation of two or possibly three absorption bands in the crystals. These bands occur at peak energies equal to 5.45, 4.28, and 3.08 eV; the two larger bands occurring at 5.45 and 3.08 eV have also been reported by Hunt and Schuler (*7*) for X-ray irradiated Al_2O_3. However, no attempt to correlate these absorptions with any of the underlying defects was attempted by these investigators.

The purpose of the present study was to systematically investigate the effect which gamma-ray radiation has on nominally "pure" Czochralski-grown Al_2O_3 crystals, and on crystals to which iron impurities have been added with the specific goal of identifying the underlying features of the defect structure responsible for the paramagnetic absorption previously observed (*4*) in gamma-ray irradiated alumina oxide, and, if possible, to relate these features to the optical absorption bands measured in the Al_2O_3 specimens. In particular, it was hoped that it might be possible to assign optical absorption bands in Czochralski-grown aluminum oxide crystals to impurities in particular valence states, to hole centers, or to trapped electron centers in these crystals.

Crystal Structure of Alumina

Because of the sensitivity of the paramagnetic resonance experiment to the crystalline surroundings of the paramagnetic species, it is important to describe the crystalline environment for the defect as precisely as possible. Previous investigations have shown that the basic crystal structure is rhombohedral (*8*, *9*), although the crystal may be viewed as the hexagonal close-packing of oxygen ions with aluminum ions occupying two out of three interstitial sites along the crystalline c-axis. Electrostatic forces between the Al^{3+} and O^{2-} ions reduce the size of the shared triangles and slight distortion in the hexagonal close-packing results. This distortion results in a slight enlargement and rotation about the c-axis of the adjoining oxygen triangles. The measurements of Newnham and

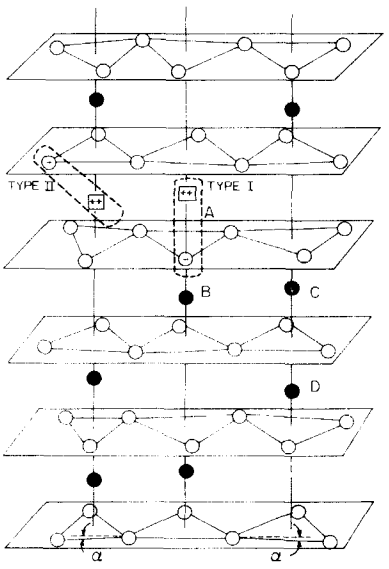

FIG. 1. The crystal lattice of aluminum oxide. *A*, *B*, *C*, and *D*, indicate the four nonequivalent aluminum ion sites. A paramagnetic trapped-hole-impurity complex defect is also shown.

DeHaan (*8*) yield a value of approximately 3° for this angle of rotation.

Ignoring for the moment the type I and II defects depicted, Fig. 1 shows the pairs of Al ions which are surrounded by trigonally distorted octahedra of oxygen ions. This figure represents stacking of these Al_2O_3 molecules along the *c*-axis of the crystal. The aluminum–oxygen distance for one of the oxygen triangles is given by 1.969 Å, while the other triangle of each octahedron is larger and lies closer to the Al atom with an aluminum–oxygen distance of 1.856 Å. In this model, every third octahedral interstice along the *c*-axis is a natural void with both oxygen ion triangles rotated in the same way.

Geschwind and Remeika (*9*) note that, in the corundum lattice, the Al^{3+} ion is in octahedral oxygen coordination. This octahedron is not regular but is severely distorted along a threefold direction which coincides with the *c*-axis of the crystal. The point symmetry of the aluminum site is given as C_3, while the point symmetry of the oxygen ion site is given as C_2.

Artman and Murphy (*10*) note that there are four inequivalent Al sites per unit cell and that the Al_2O_3 unit cell is composed of twelve Al^{3+} ions and eighteen O^{2-} ions. However, the four sites are related through an inversion center and, therefore, the symmetry considerations result in only two magnetically inequivalent cation sites with respect to the crystalline field.

Experimental

Nominally pure single crystal specimens of Czochralski-grown and vapor-phase grown Al_2O_3 specimens were obtained for the measurements made in this investigation. Vapor phase specimen No. 300 was obtained from the National Bureau of Standards and was mounted on a goniometer and oriented by a back-reflection Laue technique so that a single crystal sample $2 \times 5 \times 6$ mm^3 could be cut from the crystal with the crystalline *c*-axis perpendicular to the 6 mm face.

The remaining specimens used in this investigation were Czochralski-grown Al_2O_3 crystals obtained from the Linde Crystal Products Division of the Union Carbide Corporation. Each as-received sample was $\frac{1}{2}$ in. diam. × 0.02 in. thick and was oriented with a *c*-axis perpendicular to the crystal face. An analysis supplied by the manufacturers of the "as received" samples obtained from both sources is given in Table I.

TABLE I

SPECIMEN IMPURITY CONCENTRATION

Impurity	Concentration[a] (ppm by wt.)	Paramagnetic ion[b] concentration (ppm by wt.)
Pb	10–15	—
Ga	5–10	—
Fe[c]	5.0 (< 4[d])[c]	(Fe^{3+}) (0.1–1.0)
Si[c]	10–25 (< 10[d])[c]	—
Cu[c]	0.04	—
Ca	tr	—
Mg	tr (< 1[d])[c]	—
Cr[c]	tr (< 1[d])[c]	(Cr^{3+}) (0.12–1.7)
Mn[c]	0.0005	Not Detected
Ir[c]	0.002	—
Sc[c]	0.015	—

[a] Determined by spectrochemical or neutron activation analysis on representative specimens.

[b] Determined experimentally by ruby standard comparison of integrated paramagnetic absorptions.

[c] Indicates impurity found in N.B.S. vapor-phase grown Al_2O_3.

[d] Indicates the detection limit, not necessarily the concentration in the specimens.

Iron-doped samples were prepared using a high-temperature diffusion technique. Single crystal samples of Czochralski-grown Al_2O_3 were hung in a dense alumina crucible above and out of contact with a supply of iron oxide powder so that the Fe-dopant could be introduced into the Al_2O_3 sample by diffusion from the vapor phase. A second, slightly larger alumina crucible, was used as a cover and this entire system was set on an alumina pedestal within the furnace so that the sample was centered within the tungsten heating element of the furnace. Temperatures at the crucible were measured with a W vs W + 26% Re thermocouple which was tantalum-sheathed.

After removing the samples from the furnace following a diffusion-doping run, some surface coloration was noted in each specimen, the color usually ranging from a pale to light green. Microscopic examination after diamond grinding indicated that this surface coloration had not penetrated the total thickness of the speciman. The samples were ground and polished with diamond paste until all visible coloration had been removed. The polished specimen was than placed in a clean, high-density covered alumina crucible and placed in the resistance furnace for a homogenization anneal. To assure homogeneity of the doped sample, it was heated at 1800°C for periods from 4 to 5 days.

In order to induce paramagnetic defects in the specimens, a tubular ^{60}Co source of 146,000 Ci, located at the Argonne National Laboratory, was used. The source was composed of eight tubular rods arranged in a square pattern of approximately 9 in. and were connected to a motorized hoist so that they could be raised and lowered into position automatically.

To establish the dose rating resulting at various distances from the ^{60}Co source, Fricke solution (*11*) and cobalt glass (*12*) dosimetry were used to establish the radiation level (in rad/hr) at the position of the samples. Fricke solution consisting of 1 mole Fe SO_4 in an 8 *N* aqueous solution of H_2SO_4 has been studied extensively at Argonne for determining radiation field intensities and was chosen as the primary standard for calibrating the intensity levels for the ^{60}Cobalt facility (*12*).

The doses reported in this investigation are the measured values in air at the position where the sample was located, not the ionization in the samples. Gamma rays emitted by ^{60}Co are 1.1 and 1.3 MeV, but the energies incident on the specimens will be somewhat less due to the Compton scattering in the Co. All of the irradiations were performed at liquid nitrogen temperatures. To assure that neither thermal nor optical bleaching could occur in the specimens, they were enclosed in aluminum foil before the irradiation and transported to the Argonne Laboratory in a liquid nitrogen dewar. After irradiation, the specimens were stored in liquid nitrogen. Any subsequent sample handling was done in subdued light and as close to liquid nitrogen temperature as possible.

The EPR measurements were performed at *x*-band frequencies using a conventional Varian E-4 spectrometer. Some preliminary measurements, however, requiring higher magnetic fields were obtained using a Bruker B-ER 414/418, *x*-band spectrometer. The crystal sample holder used was designed to mount above the magnetic poles of the magnet of either spectrometer. Samples were affixed to flat surfaces ground on quartz tubes. Several measurements of the mounting cements and sample rods were performed to determine the possible contributions to the ESR spectra which might occur after irradiation of these materials. Two of the mounting cements used in this investigation (Ply-bond and Sauereisen cements) were found to result in several radiation-induced EPR spectra which occurred at *g*-values significantly separated from the observed defect spectra. Interference with this observed defect spectra and the absorptions caused by irradiating the mounting cement were seen to occur for several orientations of the specimens. However, for the specimen orientations reported in this investigation interference absorptions from the mounting cement were not significant. All the specimen tubes were mounted onto a nylon goniometer head which acted as the axis of rotation. The angular variation of this rotation head was determined using a circular protractor calibrated in degrees, while a vernier mounted below this protractor was calibrated to read to 0.1°. The absolute accuracy of angular measurement could be determined to within $\frac{1}{2}$°.

The *c*-axis of the specimens was usually mounted perpendicular to the axis of rotation of the sample goniometer, while the axis of rotation was parallel to an *a*-axis of the hexagonal crystal, thus allowing both parallel ($H \parallel c$) and perpendicular ($H \perp c$) positioning of the crystal *c*-axis with respect to the applied magnetic field. The azimuthal angle which the *c*-axis made with the magnetic field was determined by the angle to which the quartz rod had been ground and could vary over a limited range of about 10 degrees depending on

the sample length. The entire sample holder was designed to allow either a liquid nitrogen dewar or a variable temperature apparatus to be mounted within the x-band cavity of the spectrometer. For this investigation, however, only liquid nitrogen temperature spectra have been reported.

Relative concentrations of the paramagnetic centers observed in this investigation were obtained using numerical double integration computer techniques (*13*, *14*). The observed EPR resonance line was compared directly with the resonance line attributed to Cr^{3+} absorption in samples which had previously been calibrated against primary ruby EPR standards. The Cr^{3+} absorptions were chosen as primary and secondary concentration standards because of the similarity of the crystal environment and previous use of ruby as EPR standards (*15*).

The optical absorption measurements reported in this investigation were obtained using a Zeiss MM12 monochrometer. This instrument is a double-pass monochrometer designed with interchangeable quartz or glass prisms allowing a large wavelength region to be investigated. In order to observe the absorption spectra at liquid nitrogen temperatures, the radiation leaving the monochrometer was passed through a Quanta Laboratories Collimator (Model A12-15) and directed at a liquid nitrogen, cold-finger sample holder. The Zeiss detector system used in this investigation consisted of a RCA 1P28 photomultiplier tube which received incident intensity through a system of internal optics and mirrors. This detector was mounted on a movable base so that it could be positioned to measure the intensity through either the sample or reference channel at the same wavelength.

Results

EPR spectra observed for the nominally "pure", as-received Al_2O_3 specimens, were characteristic of the Fe^{3+} and Cr^{3+} ion absorptions previously observed (*16*, *17*) for these ions in substitutional cation sites. The relative concentration of these transition metal impurity ions was determined by comparisons

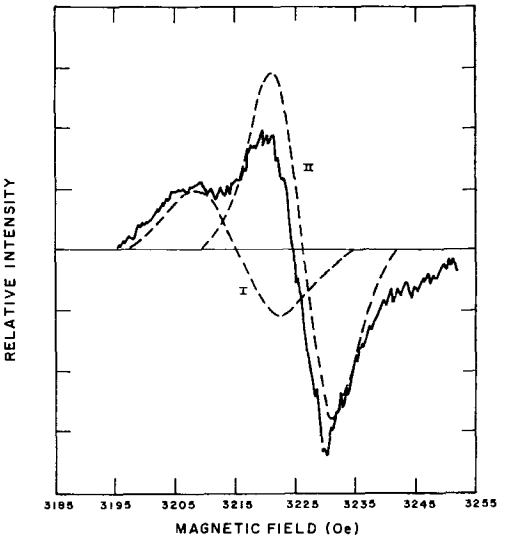

FIG. 2. Radiation induced EPR spectrum for as received Al_2O_3 after 10^5 rad ^{60}Co irradiation, c-axis perpendicular to Zeeman magnetic field.

with the previously calibrated ruby EPR standard, and the average impurity concentration for three different as-received specimens are listed in Table I. Variations in the concentration of these paramagnetic impurities from sample to sample were found to be negligible.

When the as-received specimens were subjected to various dose levels of ^{60}Co gamma-ray radiation (10^4–10^7 rad), a small anisotropic EPR resonance resulted (see Fig. 2). The radiation-induced resonance did not show any significant differences from sample to sample with respect to line-shape or spectroscopic g-values. However, the line-shape and the spectroscopic g-values for the observed resonance line were found to be slightly dependent on specimen orientation with $g_{\parallel} = 2.012$ and $g_{\perp} = 2.007$ where parallel and perpendicular refer to the orientation of the crystal c-axis with respect to the Zeeman magnetic field. The resonance absorption line appears particularly well resolved when the crystal is in the perpendicular orientation ($\theta = 90°$, $\phi = 90°$).[1] The line width at this

[1] With the magnetic field vector directed along the x-axis of a right-hand Cartesian coordinate system, θ and ϕ are the azimuthal and polar angles which define spatial position of c-axis of the crystal.

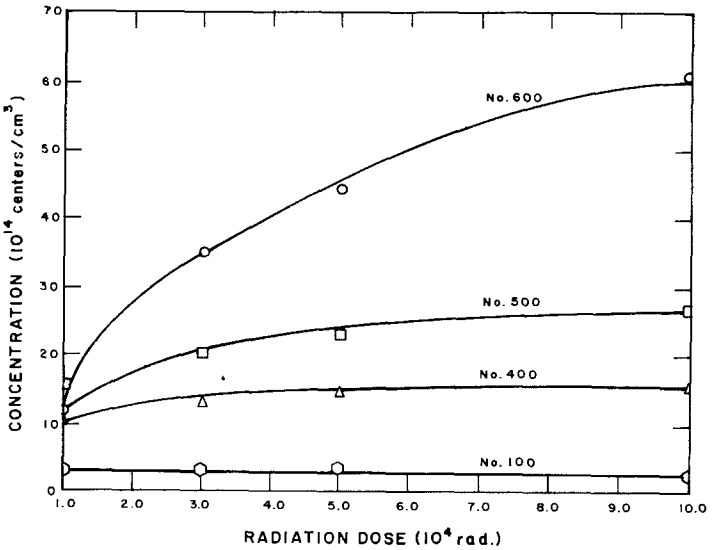

FIG. 3. Variation of radiation induced EPR center concentration as a function of radiation dose for as received and iron-doped Al_2O_3.

orientation was found to be approximately 45 Oe. For a particular orientation, the intensity remained relatively constant as a function of power level but decreased significantly as a function of increasing temperature.

The integrated intensity of the radiation-induced absorption line observed as a function of radiation dose for as-received specimen No. 100 is shown in Fig. 3. The relative concentration observed in various other Czochralski-grown, as-received samples was found to be in approximate agreement with the integrated intensity observed for this specimen.

In order to determine the effect that the iron impurity had on the radiation-induced EPR absorption line, the EPR spectra observed for iron-doped Al_2O_3 specimens were recorded after the specimens had been prepared as previously described. Except for additional intensity increases attributed to the fine structure absorption lines identified as due to the Fe^{3+} trace impurity in the crystals, no other changes were observed in any of the

TABLE II

TOTAL CONCENTRATION OF EPR CENTERS

Sample number	Sample condition	Cr^{3+} (spins/cm^3)	Fe^{3+} (spins/cm^3)	Radiation Induced Centers by 10^4 rad (spins/cm^3)	3×10^4 rad (spins/cm^3)	5×10^4 rad (spins/cm^3)	10^5 rad (spins/cm^3)
100	As received	7.92×10^{16}	4.36×10^{16}	3.18×10^{14}	3.39×10^{14}	3.41×10^{14}	3.74×10^{14}
200	As received	7.28×10^{16}	5.0×10^{16}	2.96×10^{14}	3.09×10^{14}	3.67×10^{14}	
300	As received	5.76×10^{15}	5.04×10^{15}	—		—	
400	Fe-doped at 1350°C	7.15×10^{16}	6.22×10^{16}	1.12×10^{15}	1.21×10^{15}	1.42×10^{15}	1.57×10^{15}
500	Fe-doped at 1550°C	7.99×10^{16}	1.42×10^{17}	1.56×10^{15}	1.18×10^{15}	2.25×10^{15}	2.68×10^{15}
600	Fe-doped at 1800°C	8.27×10^{16}	1.15×10^{18}	1.12×10^{15}	3.45×10^{15}	4.38×10^{15}	6.1×10^{15}

samples containing iron after diffusion doping. A careful examination, using both high and low power microwave levels in the magnetic field regions not showing EPR resonance lines, indicated that no new features in the EPR absorption spectra attributable to other paramagnetic impurities or defects could be detected. The relative concentration of the Fe^{3+} impurity introduced into the samples was determined by comparison with the previously calibrated Cr^{3+} absorption lines occurring in the samples. These concentrations are listed in Table II.

The iron-doped samples were gamma-ray irradiated, starting at dose rates ranging from 10^4 to 10^7 rad, and the EPR spectra were recorded, with special interest centering around the magnetic field value for which the previous radiation induced resonance line for as-received samples was recorded. For these doped samples, progressively increasing radiation doses resulted in a radiation-induced EPR resonance line which increased to a saturation level with increasing radiation dosage as shown in Fig. 3. The radiation-induced resonance absorption line observed for specimen No. 600 is shown in Fig. 4, while Figs. 5 and 6 represent the observed EPR absorption for other orientations of this specimen in the Zeeman magnetic field.

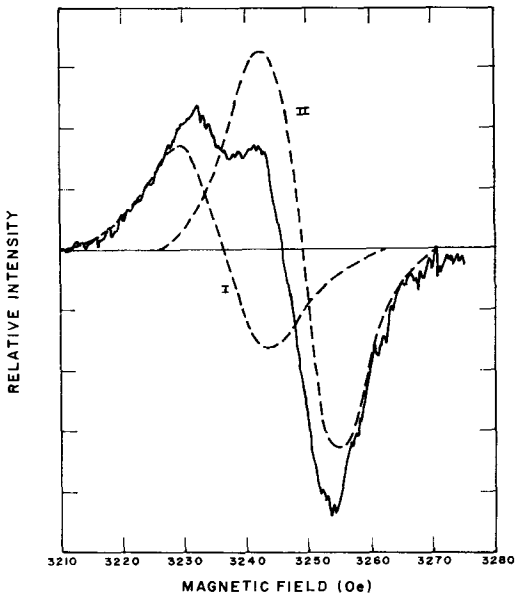

FIG. 4. Radiation induced EPR spectrum for specimen No. 600 after 10^5 rad ^{60}Co irradiation, c-axis perpendicular to Zeeman magnetic field.

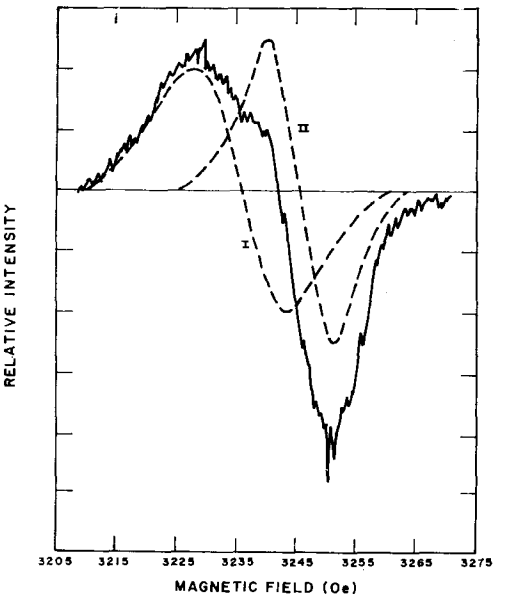

FIG. 5. Radiation induced EPR spectrum for specimen No. 600 after 10^5 rad ^{60}Co irradiation, c-axis at 40° to the Zeeman magnetic field.

The line-shape and spectroscopic g-values of this absorption line were found to be similar to the values observed for as-received Al_2O_3 which had been irradiated to saturation gamma-ray radiation doses. The significance of the observed EPR spectra is apparent, however, in Fig. 3 where the intensity of the observed resonance line can be seen to increase with increasing Fe^{3+} concentration in the specimens.

Standard optical transmission measurements for nominally pure as-received and Fe-doped Al_2O_3 specimens were also performed in this investigation. Optical absorption measurements on the Czochralski-grown, as-received specimens studied in this investigation at liquid nitrogen temperature, indicated that four or possibly five very weak absorption shoulders may be identified in the energy regions around 2.2, 3.1, 4.8, 6.4, and possibly 7 eV. Previous measurements (*18*) have identified optical absorption peaks occurring

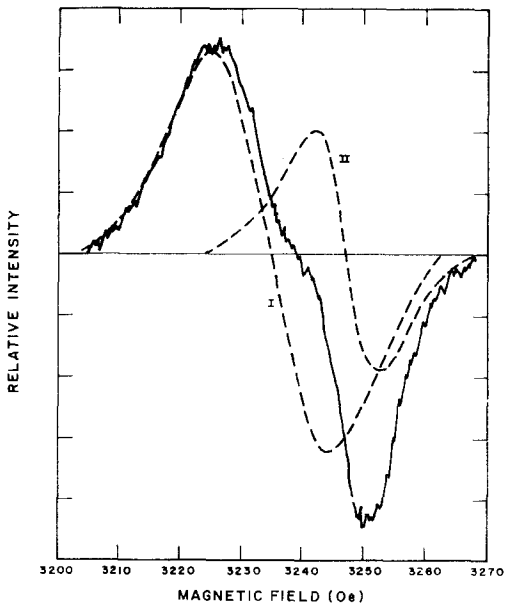

FIG. 6. Radiation induced EPR spectrum for specimen No. 600 after 10^5 rad ^{60}Co irradiation, c-axis at 10° to the Zeeman magnetic field.

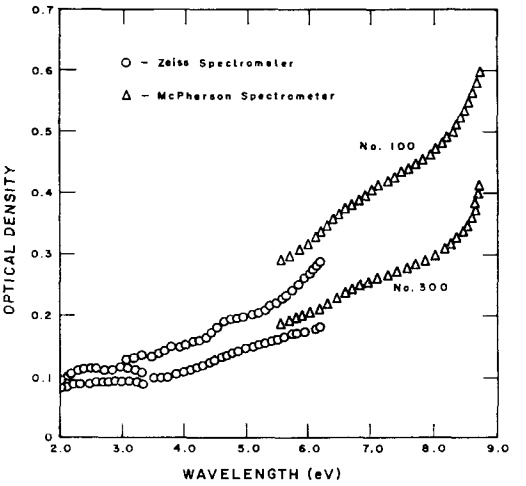

FIG. 7. Optical absorption in as received Al_2O_3.

at 2.24 and 3.1 eV as strong impurity transitions occurring because of Cr^{3+} impurity atoms in the Al_2O_3 lattice. Similar optical results (*19*) for Fe^{3+} in Al_2O_3 indicate that weak transitions for this ion are found at 4.8, 6.4, and 6.9 eV. Thus, the absorptions measured for our as-received specimens are probably related to the presence of these impurity atoms in the as-received crystals.

As shown in Fig. 7, optical transmission measurements on all the as-received specimens used in these investigations were found to be very uniform and showed little variation from sample to sample. In the energy range studied in this work, the optical density of these specimens was found to be no greater than 0.4 until reaching the intrinsic absorption edge at 8.8 eV.

Because of the relatively low intensities of the radiation-induced defect centers expected to occur in this investigation, optical difference spectra between the "pure" and irradiated doped crystals and the as-received crystals were recorded here. Pure, as-received Al_2O_3 did not reveal any radiation-induced optical absorption, even after being subjected to a 10^7 rad dose of gamma-ray radiation. In the case of iron-doped samples, however, significant changes in the optical absorption difference spectra were observed as indicated in Fig. 8. For specimen No. 600, the optical absorption peaks occurring at 4.84 eV and the absorption edge at 6.2 eV may have appeared because of the difference in Fe^{3+} concentration between the standard and doped samples.

The two remaining peaks at 3.08 and 5.44 eV are observed because of some unspecified ionization process which occurs when the doped samples are subjected to gamma-ray radiation. These optical absorption peaks occurring at 3.08 and 5.44 eV have been previously measured in Verneuli-grown Al_2O_3 (*6*). The peak positions measured for our doped specimens appear to be in general agreement with these earlier measurements. However, the half-widths of the Gaussian absorption peaks which were fit to the observed spectra were found to be slightly greater than one-half of the values reported by Levy (*6*) for his room-temperature measurements.

To estimate the number of centers giving rise to the observed optical absorptions occurring after the specimens were irradiated, Smakula's formula (*20*), relating the number of centers to the intensity of the observed absorption band, was applied to the Gaussian absorption bands fit to the absorption peaks occurring at 3.08 and 5.44 eV. Assuming that

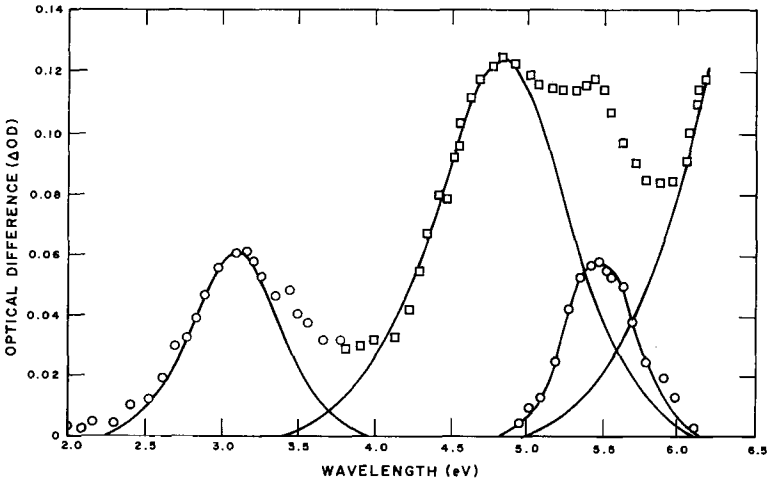

FIG. 8. Optical difference spectra observed for specimen No. 600 after 10^5 rad ^{60}Co irradiation.

the oscillator strength is unity, the number of centers giving rise to these observed optical absorption bands was estimated to be 1.7×10^{15} and 1.08×10^{15} centers/cm^3, respectively. Both these concentrations are in general agreement with the number of defect centers measured for specimen No. 600 using EPR techniques.

To determine whether a significant correlation exists between the observed optical absorptions and the EPR measurements, a series of thermal annealing experiments were performed on sample No. 600. Specimen No. 600 was first annealed in vacuum at 1600°C and slow cooled to room temperature to establish a reference condition for comparison purposes. The effect of this treatment was to reduce the induced-EPR absorption below the detectable limits of the spectrometer. A similar reduction occurred for the optical absorption peaks at 3.08 and 5.44 eV.

The specimen was then irradiated to a 10^7 rad dose level using ^{60}Co gamma rays. EPR and optical resonance spectra were determined on this sample at liquid nitrogen temperature. Thermal-bleaching of the sample was accomplished by using a hot oil bath, the annealing temperature being measured with a thermometer. Warm-up and cool-down times for the sample were expected to be relatively fast because of the small sample size and the relatively short transfer times from the nitrogen dewar to the oil bath. The thermal-bleach temperature was 100°C and the anneal of the irradiated specimen was interrupted after various time intervals so that the optical and EPR spectra could be recorded at liquid nitrogen temperature. The relative concentrations of the optical absorption peaks occurring at 3.08 and 5.44 eV, along with the relative intensity of the EPR resonance line determined by double integration techniques, are shown in Fig. 9 as a function of annealing time. The normalized change in line intensity (proportional to defect concentration) as a function of annealing time is listed in Table III. From

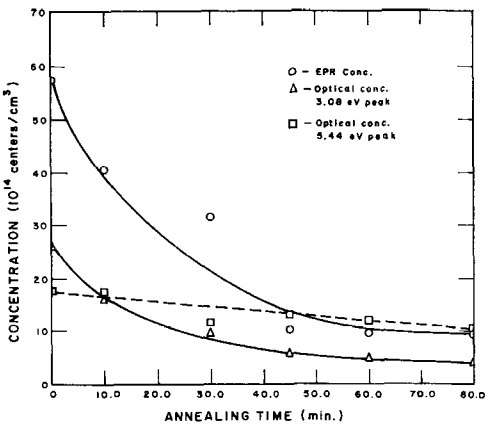

FIG. 9. Variation of optical and EPR intensities induced by gamma-ray radiation as a function of thermal bleaching time.

TABLE III

NORMALIZED INTENSITY VALUES FOR RADIATION INDUCED PEAKS

Time at anneal temperature (min.)	Intensity of ESR defect center	Intensity of 3.08 eV Optical peak	Intensity of 5.44 eV Optical peak
No Anneal	100	100	100
15	70.5	60.5	100
30	55.5	36.5	71.5
45	16.7	20.4	81.5
60	13.9	17.0	77
80	13.0	13.6	68.7

these results, it is apparent that the concentration of the center which gives rise to optical absorption occurring at 3.08 eV and that center which we associated with the observed EPR spectra decrease with increasing annealing time in about the same manner.

Discussion of Results

Since the energy associated with the gamma-ray radiation used in this experiment is much greater than the band gap of Al_2O_3, electron-hole pairs are undoubtedly created by γ-irradiation of the samples. Thus, the new paramagnetic centers observed after gamma-ray irradiations of the specimens are most likely formed by some defect which traps those charges freed during irradiation. Models for the paramagnetic defect center or centers occurring in Al_2O_3 must account for the magnitude of the g-values, the symmetry of the centers, and the observed dependence of the radiation-induced EPR absorption line on the concentration of iron impurity in the host lattice.

The lack of observable hyperfine structure in the observed absorption would tend to rule out the association of the defect center with the host aluminum ion (having a nuclear spin $I = 5/2$). Despite the fact that there is a clear dependence of the intensity of the radiation-induced absorption spectra on the iron impurity content in the samples, the observed spectra is not compatible with that for the Fe^{3+} ion alone or for any other paramagnetic metal ion commonly occurring in an Al_2O_3 crystal. Furthermore, this spectra could not be directly associated with other ionization states of the iron impurity ions, since EPR absorption spectra would not be observable for the high spin Fe^{2+} or Fe^{4+} ions in the crystalline field associated with the cation lattice sites in Al_2O_3.

The possibility that the observed spectra may arise from the ozonide radical has also been considered. If such a radical did exist it is apparent that the geometry of the Al_2O_3 lattice would tend to produce such a radical in the oxygen ion lattice plane of the Al_2O_3 crystal. A model of the ozonide ion in this lattice would thus result in the unpaired electron occupying the p_x orbital perpendicular to the O_3^- plane and parallel to the crystalline c-axis.

The experimental results, however, indicate that the observed g-value for this crystal orientation in the specimen magnetic field is much greater than the g-value measured for the ozonide radical in other crystal systems (*21*). Furthermore, the orientation spectra for the EPR spectra observed in the Al_2O_3 crystals does not correspond with results observed for the EPR spectra characteristic of the ozonide radical in other crystalline materials (*22*).

Because the magnitude of the g-values associated with the radiation-induced EPR spectra observed in this investigation are in reasonably good agreement with the measured values reported by Gamble et al. (*4*) a detailed examination of the tentative centers proposed by these authors is warranted.

From the results of this investigation (see Fig. 3), it is apparent that the intensity of the radiation-induced resonance line can be significantly influenced by the iron impurity content in the host crystal. Indeed, the present results suggest that any defect model describing the observed EPR spectra must involve the existence of defect complexes containing cation impurity ions in the host crystal. This result precludes the tentative identification of the underlying defect mechanism responsible for the radiation induced EPR spectra as due to cation and anion lattice vacancies acting as either electron or hole traps in the Al_2O_3 lattice.

An extrinsic defect model proposed by Gamble et al. (*4*) which consists of a hole localized at an anion next to a charge-deficient cation site (e.g., a defect complex) where the cation site is occupied by a monovalent or divalent impurity atom should be examined to determine whether it is consistent with the present experimental evidence. If a monovalent or divalent impurity is introduced into the crystal as is required by the Gamble model, the charge-neutrality condition dictates that an appropriate number of compensating anion vacancies must also be introduced into the host crystal. A second, somewhat different, defect complex having properties identical to the above complex can also result when trivalent substitutional impurities are introduced in the Al_2O_3 host crystal. As shown below, this defect complex involves the transfer of an electron from an oxygen ion to an adjacent Fe^{3+} impurity ion, with the result that a hole may be localized next to a charge-deficient Fe^{2+} impurity.

Using the Kroger–Vink (*23*) notation, the defect complex which is introduced in the Al_2O_3 lattice by the gamma-ray irradiation can be written as:

$$Fe_{Al}^{x} + O_0^{x} \xrightarrow{h\nu} (Fe_{Al}O_0)^{x}$$

Since the formation of a defect center of this type would be expected to result in a decrease of Fe^{3+} ion concentration, a correlation of decreasing Fe^{3+} concentration with increasing $(Fe_{Al}O_0)^{x}$ complex concentration might be anticipated. Unfortunately, because of the relatively small concentration of defect complexes found with respect to iron impurity concentration in our samples (see Table II), it was not possible to establish a quantitive relationship between the defect complex and Fe^{3+} concentrations.

Evidence for the existence of the defect complex as described above, however, may be obtained from several other considerations. An examination of the crystalline structure of Al_2O_3 shows that such a defect complex would result in an axially symmetric center where the principal axis is directed along a line joining the 0^{-1} ion to the Fe^{2+} impurity ion. From the symmetry of this defect, it is easily seen that six orientations with respect to the principal c-axis of the crystal would result. Moreover, when the possibility of the two magnetically inequivalent cation sites is taken into consideration, a total of twelve resonance absorption lines should be expected for this type of defect.

For the specific specimen orientation where the Zeeman magnetic field is directed perpendicular to the c-axis of the crystal ($\theta = 90°$, $\varphi = 90°$) two types of defect orientation result as shown in Fig. 1. In order to simplify the discussion, the 3° rotation of the oxygen ion triangles in the host crystal is disregarded. In this case, Type I orientations of the defect complex will have their principal symmetry axis perpendicular to the applied magnetic field, and there will be two equivalent Type I orientations possible in this simplified model. Similarly, Type II orientations of the defect complex $(Fe_{Al}O_0)^{x}$ will occur at an angle φ relative to the applied magnetic field and four equivalent Type II orientations will be possible in the host crystal. Under these conditions, two EPR resonance lines would be expected to occur for this defect. Resonance for defects having a Type I orientation would be expected at a g-value denoted by $g_\perp$ for the defect, where $\perp$ refers to the perpendicular orientation of a line joining the Fe^{2+} and O^{-1} ions and the applied magnetic field. A resonance line for defects having Type II orientations would be expected to occur also; however, because of their orientation, the resonance line will be shifted away from the $g_\perp$ value and occur at a value g_ρ which is somewhere between $g_\perp$ and $g_\parallel$ for the defect complex where ρ is the angle between the principal axis of the defect and the applied magnetic field.

Relaxing the angular restriction placed on the oxygen–ion triangles will result in a slight shifting of the defect complex with respect to the applied magnetic field and some line broadening of the observed resonance lines will occur. Similarly, because two magnetically inequivalent cation sites are present in the host lattice, the existence of a total of four Type I defects and eight Type II defects is possible in the host crystal.

Because of the relatively small contribution which might be expected from a slight misalignment of the complex defect, it is reason-

able to approximate the observed EPR resonance line by two derivative Gaussian absorption lines having g-values and intensities consistent with the simplified crystal model. However, the peak-to-peak half-widths of the component lines will be influenced by the slight misalignment of the defects and the concurrent broadening that results.

In attempting to devise a mathematical model which would describe the observed EPR spectra for the perpendicular orientation alluded to above, it was assumed that two Gaussian derivative component absorption lines could be used to explain the observed EPR spectra. Component I would be composed of four axial $(Fe_{Al}O_0)^x$ defects each having approximately a Type I orientation. Component II will be composed of eight $(Fe_{Al}O_0)^x$ defects, each with approximately a Type II orientation.

In order to test whether the observed spectra could be reasonably well fit by the above model, a nonlinear, least-squares computer program was adapted to fit the two derivative Gaussian absorption curves having the form:

$$dy(H)/dH = \exp(\tfrac{1}{2})B(1) \times \left[\frac{H - B(2)}{B(3)}\right] \exp\left[-\tfrac{1}{2}\left(\frac{H - B(2)}{B(3)}\right)^2\right]$$

to the experimentally observed data. Here $B(1)$, $B(2)$, and $B(3)$ are adjustable parameters related to the magnitude, position, and peak-to-peak half-width of the Gaussian absorption peak as follows.

$$B(1) = \frac{dy_m}{dH}, \qquad B(2) = H_0, \qquad B(3) = \tfrac{1}{2}\Delta H_{pp}$$

where ΔH_{pp} is the difference in magnetic field on the derivative curve, y_m the maximum

TABLE IV

CHARACTERISTIC g-VALUES, PEAK WIDTHS, AND INTENSITIES FOR GAUSSIAN ABSORPTION COMPONENT LINES DESCRIBING THE OBSERVED EPR RESONANCE IN IRRADIATED Al_2O_3

Specimen No.	Orientation	Component line	g-value	ΔH_{pp}[a]	Intensity[b]
100	$\theta = 90$	0	2.006		
(as received)	$\phi = 90$	I	2.011	12.8	6.9
		II	2.004	10.2	13.1
	$\theta = 90$	0	2.006		
500	$\phi = 90$	I	2.013	12.1	8.1
		II	2.005	11.6	19.5
	$\theta = 90$	0	2.008		
600	$\phi = 90$	I	2.015	13.5	13.6
		II	2.007	12.2	20.6
	$\theta = 40$	0	2.011		
600	$\phi = 90$	I	2.016	15.5	20.5
		II	2.009	11.5	14.1
	$\theta = 10$	0	2.012		
600	$\phi = 90$	I	2.015	19.5	53.6
		II	2.008	10.5	9.4
Average		0			
g-values		I	2.014		
		II	2.007		

[a] ΔH_{pp} = the peak to peak width of the Gaussian derivative absorption line.
[b] These values have been normalized to unity gain factor.

intensity of the absorption curve, and H_0 the value of the magnetic field occurring at that maximum.

The computer program used in this investigation was a modified version of the program originally developed by Marquardt (*24*). The program has been designed to adjust the B parameters of the above model to minimize the sum of the squares of the residuals defined by

$$\Phi = \sum_{i=1}^{n} (y_i - \hat{y}_i)^2$$

where y_i represents the ith observed data point and $\hat{y}_i$ represents the data point predicted by the mathematical model. In the present instance, the amplitudes, line-widths and line positions of two derivative Gaussian components were allowed to vary in this program, and the "best fit" B parameters for both component lines were obtained for all the specimens studied.

Resonance lines computer-fitted to the radiation-induced EPR spectra for some of the present specimens are shown in Figs. 2 and 4. In addition, the resonance line positions, half-widths and normalized intensities of the computer-fit component resonance lines are listed in Table IV. For the perpendicular orientation ($\theta = 90°$, $\varphi = 90°$) the intensities of the two Gaussian component absorption lines are seen to be in relatively good agreement with the intensity predicted by the defect model proposed here. The g-values of the component absorption lines determined by computer-fitting are in reasonable agreement with the g-values measured for hole-type defects in other oxide materials (*25*). Furthermore, the influence of the Fe^{3+} impurity content on the intensity of the radiation-induced EPR spectra is consistent with the defect complex proposed here, since increases in Fe^{3+} impurity in the host crystals would create a larger number of trapping sites for the electrons freed from the oxygen ions during the irradiation.

Since the defect complex described above can be considered to behave identically to the previous complex proposed by Gamble (*4*), the observed EPR spectra was also analyzed under the assumption that the impurity introduced into the host crystal was either monovalent or divalent cation substitutional before the samples were gamma-ray irradiated. Under this condition a second charge-trapping site is introduced into the host crystal (i.e., an anion vacancy) and the experimental EPR spectra observed for the specimen after gamma-ray irradiation should include a resonance due to an electron transferred to the anion vacancy trap as well as a hole localized next to the charge deficient cation site (mono- or divalent impurity). Therefore, an attempt was made here to computer-fit the observed data using a Gamble-type, three Gaussian-component mathematical model. A comparison of the fit obtained for the observed results for both our two-component model and Gamble's three-component model including the proposed resonance due to an electron trapped at an anion vacancy is shown in Figs. 10 and 11. The results as shown in these figures can be represented as the "goodness" of fit of the proposed models. Since the difference between the observed data point, y_{obs}, and the value of the data point calculated by the proposed model, y_{calc}, is plotted on the ordinate of these figures, the results depicted

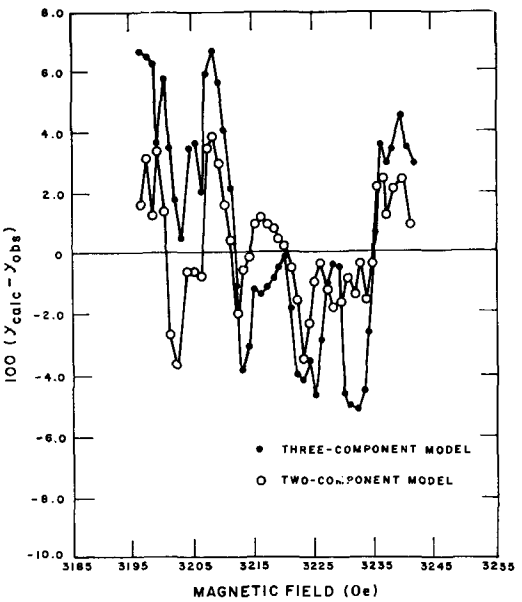

FIG. 10. Best fit variation of the two and three Gaussian component line models for computer fitting to the EPR spectra observed for specimen No. 100.

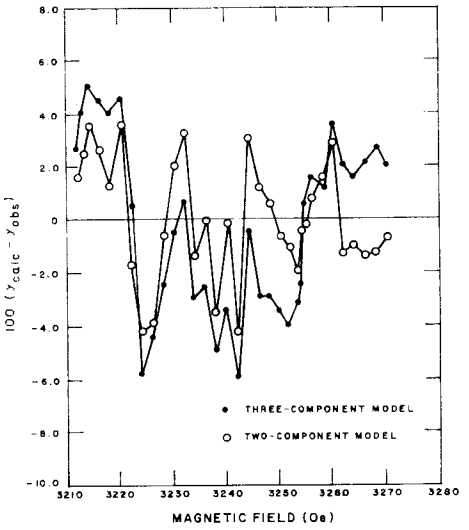

FIG. 11. Best fit variation of the two and three Gaussian component line models for computer fitting to the EPR spectra observed for specimen No. 600.

can be regarded as representing the "goodness" of fit of the two models.

A statistical analysis of the results shown in Fig. 10 indicates that the sum of the squares of the residuals for the two and three-component models was 0.026 and 0.936, respectively, indicating that: (1) the two-component model proposed here exhibits considerably smaller deviations than does the Gamble model; and (2) the deviations for the present model are randomly distributed about the exact fit value (ordinate value = 0). Thus, although possessing fewer adjustable parameters, the two-component model fits the present experimental observations better than the more complex model proposed by Gamble et al. (*4*).

Because of this improved fit of the two Gaussian components to the observed EPR spectra the inclusion of a component, as initially proposed by Gamble et al. (*4*), to account for an electron trapped in an anion vacancy is not considered to be necessary and thus the EPR spectra which results after the gamma-ray irradiation of the iron-doped crystal is considered to be due solely to a hole localized at an anion next to a divalent Fe impurity as discussed above.

Perhaps the most significant result of this investigation is the correlation between the 3.08 eV optical absorption band and the trapped hole-center, tentatively identified from the EPR observations. However, because of the relatively low-intensity EPR absorptions and small optical absorption bands arising from the radiation-induced centers, the concentrations of these centers, as determined here, must be considered to be rather uncertain.

Even though a definite correlation between the optical and EPR absorptions is indicated by the present results, it is still difficult to determine the underlying cause of the optical absorption band occurring at 3.08 eV, since it could arise from the O^{-1} ion in an axial crystalline field or from the Fe^{2+} impurity ion considered to be adjacent to the trapped hole. Both types of defects could give rise to the optical absorption spectra and both defects might be expected to follow the decreasing intensity of the EPR spectra which has been attributed to the $(Fe_{Al}O_0)^x$ defect complex. Further evidence for the correlation of the 3.08 eV optical absorption band and the O^{-1} ion in the Al_2O_3 lattice has been presented by Bartram et al. (*26*). In this connection, these authors have shown that the $2p$ orbitals of the O^{-1} ion split into one lower level and two upper level energy bands which are related through the spin orbital coupling constant for the defect under consideration. This relation can be given as

$$g_\perp = g_e - \frac{2\lambda}{\Delta}$$

where Δ represents the energy separation for the two levels, g_e the free electron g-value, and λ represents the spin orbital coupling of the orbitals. Using the $g_\perp$ value from the computer-fitted data obtained from our two-component model, it was possible to obtain $\lambda/\Delta = -0.0058$. Next, using the value of $\lambda = -135$ obtained by Bartram et al. (*26*) for an O^{-1} ion by the extrapolation of an isoelectronic sequence of ions, results in a Δ value for a $2p$ orbital of an O^{-1} ion equal to 2.9 eV. This is in relatively good agreement with the observed 3.08 eV optical absorption, leading us to suggest that this optical absorption may be due to a trapped hole center created by ionizing radiation.

Acknowledgments

The authors wish to thank H. S. Parker of the National Bureau of Standards for supplying them with the vapor phase grown Al_2O_3 crystals, used in this investigation. We also would like to thank Dr. M. Peterson and the Center of Educational Affairs at Argonne National Laboratories for granting one of us (CFB) a guests thesis parts appointment in order to obtain the many gamma-ray irradiations performed in this investigation. The support granted by an N.S.F. Traineeship to one of us (CFB) is also gratefully acknowledged. Helpful discussions with B. Hoffman about our EPR results are gratefully aknowledged.

References

1. J. H. SCHULMAN AND W. D. COMPTON, "Color Centers in Solids", The MacMillan Co., New York (1962).
2. J. LAMBE AND C. KIKUCHI, *Phys. Rev.* **118**, 71 (1960).
3. R. H. HOSKINS AND B. H. SOFFER, *Phys. Rev.* **133**, A490 (1964).
4. F. T. GAMBLE, R. H. BARTRAM, C. G. YOUNG, O. R. GILLIAN, AND P. W. LEVY, *Phys. Rev.* **134**, A589 (1964).
5. P. W. LEVY, *Disc. Faraday Soc.* **31**, 118 (1961).
6. P. W. LEVY, *Phys. Rev.* **123**, 1226 (1961).
7. R. A. HUNT AND R. H. SCHULER, *Phys. Rev.* **89**, 664 (1953).
8. R. E. NEWNHAM AND Y. M. DEHAAN, *Z. Kristallogr.* **117**, 235 (1962).
9. W. GESCHWIND AND J. P. REMEIKA, *Phys. Rev.* **122**, 757 (1961).
10. J. O. ARTMAN AND J. C. MURPHY, *Phys. Rev.* **135**, A1622 (1964).
11. A. ANDERSON, Argonne National Laboratory Report, ANL-5819 (1957).
12. J. HOH, Private Communication, 1972.
13. C. P. POOLE, JR., "Electron Spin Resonance", Wiley, New York (1967).
14. J. E. WERTZ AND J. R. BOLTON, JR., "Electron Spin Resonance. Elementary Theory and Practical Applications", McGraw-Hill, New York (1972).
15. P. S. THOMPSON AND J. S. WAUGH, *Rev. Sci. Instrum.* **36**, 552 (1965).
16. G. S. BOGLE AND H. E. SYMMONS, *Proc. Phys. Soc. (London)* **73**, 531 (1959).
17. J. E. GEUSIC, *Phys. Rev.* **102**, 1252 (1956).
18. R. F. BLUNT, "Optical Absorption Determination of Chromium in Ruby", NBS Technical Note 565 (A. D. Franklin and H. S. Bennett, Eds.), (1971).
19. H. H. TIPPINS, *Phys. Rev.* **B1**, 126 (1970).
20. J. J. MARKHAM, "F-centers in Alkali Halides," Solid State Physics", Supplement 8 (F. Seitz and D. Turnbull, Eds.), Academic Press, New York (1966).
21. T. ANDERSON, J. R. BYBERG, AND K. J. OLSEN, *J. Phys. Chem.* **71**, 4129 (1967).
22. K. TAGAYA AND T. NOGAITO, *J. Phys. Soc. Japan* **23**, 70 (1967).
23. F. A. KROGER, "Physical Chemistry; an Advanced Treatise" (W. Jost, Ed.), Vol. 10, p. 229, Academic Press, N.Y. (1970).
24. D. W. MARQUARDT, *J. Soc. Industr. Appl. Math.* **2**, 431 (1963).
25. B. HENDERSON AND J. E. WERTZ, *Advan. Phys.* **17**, 749 (1968).
26. R. H. BARTRAM, C. E. SWENBERG, AND J. T. FOURNIER, *Phys. Rev.* **139**, A941 (1965).